High-quality single-crystal growth and unique electronic states in cerium and uranium compounds

2007 J. Phys.: Condens. Matter 19 125203

(http://iopscience.iop.org/0953-8984/19/12/125203)

IOP PUBLISHING JOURNAL OF PHYSICS: CONDENSED MATTER

J. Phys.: Condens. Matter **19** (2007) 125203 (14pp) doi:10.1088/0953-8984/19/12/125203

High-quality single-crystal growth and unique electronic states in cerium and uranium compounds

Yoshichika Ōnuki[1,2], Rikio Settai[1,7], Kiyohiro Sugiyama[1], Yoshihiko Inada[3], Tetsuya Takeuchi[4], Yoshinori Haga[2], Etsuji Yamamoto[2], Hisatomo Harima[5] and Hiroshi Yamagami[6]

[1] Graduate School of Science, Osaka University, Toyonaka, Osaka 560-0043, Japan
[2] Advanced Science Research Center, Japan Atomic Energy Research Institute, Tokai, Ibaraki 319-1195, Japan
[3] Faculty of Education, Okayama University, Tsushimanaka, Okayama 700-8530, Japan
[4] Low Temperature Center, Osaka University, Toyonaka, Osaka 560-0043, Japan
[5] Department of Physics, Kobe University, Kobe 657-8501, Japan
[6] Faculty of Science, Kyoto Sangyo University, Kyoto 603-8555, Japan

E-mail: settai@phys.sci.osaka-u.ac.jp

Received 3 January 2007
Published 6 March 2007
Online at stacks.iop.org/JPhysCM/19/125203

Abstract

We have grown many kinds of high-quality single crystals of cerium and uranium compounds and studied the Fermi surface properties via the de Haas–van Alphen experiments and energy band calculations. The quasi-two-dimensional electronic states are clarified in some compounds such as USb_2, $CeCoIn_5$, $UPtGa_5$ and most likely UIr. In a ferromagnet $CeRh_3B_2$, we have found unique electronic states with quasi-one-dimensional character.

(Some figures in this article are in colour only in the electronic version)

1. Introduction

The de Haas–van Alphen (dHvA) effect is a powerful method to determine the dHvA frequency F $(= \hbar c S_F/2\pi e)$ which is proportional to the cross-sectional area of the Fermi surface S_F, the cyclotron effective mass m_c^* and the Dingle temperature T_D $(=(\hbar/2\pi k_B)\tau^{-1})$, which is inversely proportional to the scattering lifetime τ of the conduction electron [1, 2]. In strongly correlated electron systems such as the cerium and uranium compounds, the cyclotron mass is extremely enhanced via the many-body Kondo effect. Low temperatures and high magnetic fields are necessary in detecting the dHvA oscillation because the detected dHvA amplitude is, simply expressed, proportional to $\exp\{-\alpha(m_c^*/H)(T + T_D)\}$, where α is a constant. If the conduction electron with the cyclotron mass $m_c^* = 1\ m_0$ (m_0: rest mass of an electron) is detected at $T = 1$ K, the same dHvA amplitude should be obtained at $T = 0.01$ K for the

[7] Author to whom any correspondence should be addressed.

Table 1. Uranium compounds and their properties studied by the dHvA experiments. Para, paramagnetic state; AFQ, antiferroquadrupolar ordering; F, ferromagnetic ordering; AF, antiferromagnetic ordering.

	Method	Structure	γ (mJ K^{-2} mol^{-1})	Ordering	Moment (μ_B/U)	Transition temperature (K)
UPd_3	Cz	Hexagonal	7.6	AFQ, AF	0.01	$T_0 = 7.5$, $T_1 = 6.8$, $T_2 = 4.5$
UB_2	Cz	Hexagonal	10	Para		
UB_4	Cz	Tetragonal	25	Para		
UAl_3	Flux	Cubic	47	Para		
USi_3	Cz	Cubic	12	Para		
UC	Cz	Cubic	40	Para		
$UCoGa_5$	Flux	Tetragonal	3	Para		
$URhGa_5$	Flux	Tetragonal	5	Para		
UGe_2	Cz	Orthorhombic	30	F	1.4	$T_C = 52$
UIr	Cz	Monoclinic	49	F	0.5	$T_C = 46$
UGa_2	Cz	Hexagonal	11	F	3.0	$T_C = 124$
U_3P_4	CT	Cubic	90	F	1.4	$T_C = 130$
U_3As_4	CT	Cubic	83	F	1.8	$T_C = 200$
UGa_3	Flux	Cubic	50	AF	0.6	$T_N = 67$
UIn_3	Flux	Cubic	40	AF	1	$T_N = 88$
$UNiGa_5$	Flux	Tetragonal	50	AF	0.9	$T_N = 90$
$UPtGa_5$	Flux	Tetragonal	67	AF	0.26	$T_N = 26$
UP_2	CT	Tetragonal	27	AF	2	$T_N = 204$
UAs_2	CT	Tetragonal	12	AF	1.6	$T_N = 274$
USb_2	Flux	Tetragonal	26	AF	1.9	$T_N = 203$
UBi_2	Flux	Tetragonal	20	AF	2.1	$T_N = 181$
UPt_3	Cz	Hexagonal	420	AF	0.02	$T_N = 5$, $T_{sc} = 0.55$
UPd_2Al_3	Cz	Hexagonal	150	AF	0.85	$T_N = 14.5$, $T_{sc} = 2.0$
URu_2Si_2	Cz	Tetragonal	70	AF	0.02	$T_N = 17.5$, $T_{sc} = 1.4$

conduction electron with a large cyclotron mass $m_c^* = 100\ m_0$. This is realized for $T_D = 0$ K. In other words, the low temperature of 0.01 K is meaningless in detecting the dHvA oscillation for a large $T_D = 1$–10 K. The low temperatures and high magnetic fields, together with a high-quality single crystal with T_D less than 1 K, are necessary to detect the dHvA oscillation for the strongly correlated electron systems.

Table 1 shows the uranium compounds which we succeeded in growing by using many kinds of techniques for the crystal growth [3]. The unique electronic states of these compounds are clarified via the dHvA effect.

2. High-quality single-crystal growth and unique electronic states

The technique for the single-crystal growth is classified as shown in table 1, depending on the degree of the vapour pressure of the melt. If the vapour pressure is low, the Czochralski method, which is denoted as Cz in table 1, is a powerful technique to obtain a large size of single-crystal ingot. On the other hand, the flux method (flux) and the chemical transport method (CT) are utilized for those compounds (see table 1) which have high vapour pressure.

2.1. Czochralski method

The conduction electrons with 100 m_0 were detected in several compounds such as $CeRu_2Si_2$ ($m_c^* = 120\ m_0$) [4], $CeCoIn_5$ ($m_c^* = 87\ m_0$) [5], UPt_3 ($m_c^* = 105\ m_0$) [6] and UPd_2Al_3

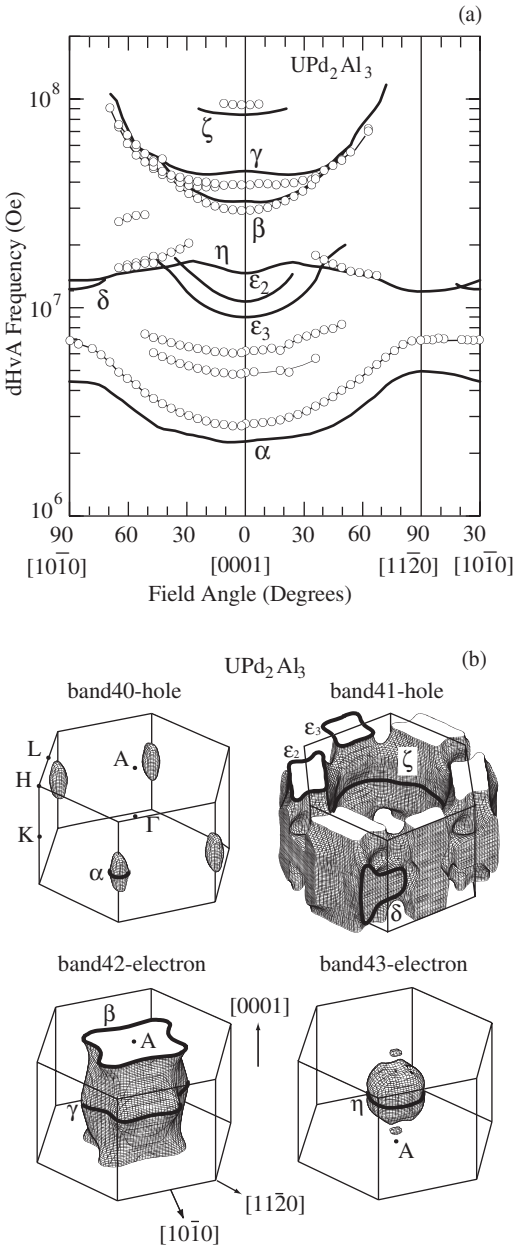

Figure 1. (a) Angular dependence of the dHvA frequency and (b) the corresponding Fermi surface in UPd_2Al_3.

($m_c^* = 65\ m_0$) [7]. In $CeRu_2Si_2$, $CeCoIn_5$ and UPt_3, a static magnetic ordering is not present, and the f-itinerant-band model is applicable for the topology of the Fermi surface, although the corresponding cyclotron mass is larger by one order of magnitude than the corresponding band mass. In UPd_2Al_3 with a Néel temperature $T_N = 14.5$ K and an ordered moment $\mu = 0.85\mu_B$/U, the 5f electrons possess a dual nature: the 5f electrons become itinerant and also contribute to the magnetic moment at the uranium site. Figure 1 shows the angular dependence of the dHvA frequency and the corresponding Fermi surface in UPd_2Al_3. Solid lines in figure 1(a) are the results of the spin-polarized LAPW band calculations. The

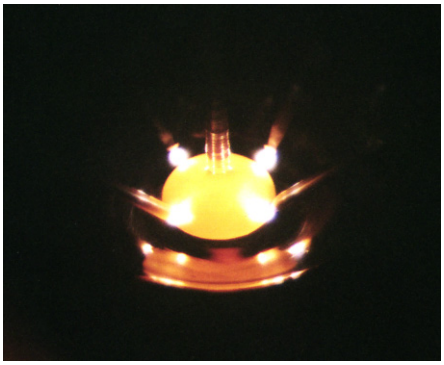

Figure 2. View of the single-crystal growth for UPt_3 in the tetra-arc furnace.

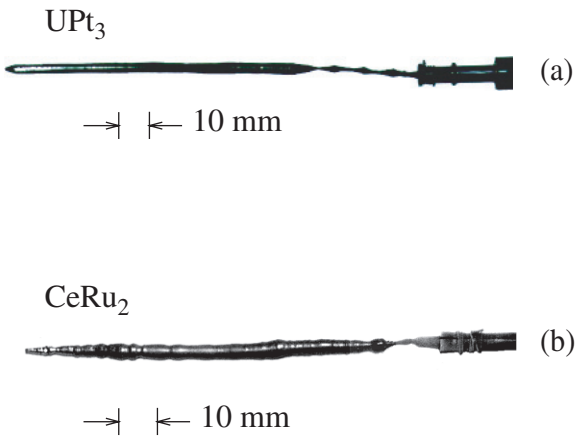

Figure 3. Single-crystal ingots of (a) UPt_3 and (b) $CeRu_2$.

experimental results are in good agreement with the band calculations [7, 8]. The spin-polarized 5f-itinerant-band model is thus applicable in UPd_2Al_3. This result is important in understanding the magnetism and electronic states in the magnetically ordered uranium compounds.

The Czochralski method was useful in growing the single crystals of UPd_2Al_3 as well as $CeRu_2Si_2$ and UPt_3. Figures 2 and 3(a) show a view of the crystal growth in a tetra-arc furnace and a single-crystal UPt_3 ingot, respectively. It is noted that there is no contamination between the melt of UPt_3 and the water-cooled Cu hearth. In particular, UPt_3 is a congruent compound with the highest melting temperature $T_m = 1700\,^{\circ}C$ in a binary U–Pt phase diagram, meaning that other binary compounds such as UPt_6, UPt_2 and UPt are not included in UPt_3. Moreover, a low vapour pressure of UPt_3 is a good condition for the crystal growth by using the Czochralski technique in the tetra-arc furnace. This method was also applied to the crystal growth for UPd_2Al_3 and $CeRu_2Si_2$.

Furthermore, a single-crystal ingot of UPt_3 was annealed under high vacuum of 10^{-10} Torr via the electrotransport method. The degas effect for impurity gases immersed in the UPt_3 ingot during the crystal growth was very effective in elevating the sample quality. It was clarified by the chemical analysis for a uranium ingot that an Fe impurity of 40 ppm in the starting uranium ingot was reduced to less than 2 ppm via the electrotransport method [9]. This annealing method was also applied to iron, where superconductivity $T_{sc} = 1$ K was observed under pressure of about 30 GPa [10].

High-quality single crystals were grown in $CeRu_2Si_2$, UPt_3 and UPd_2Al_3. For example, the residual resistivity ρ_0 and the residual resistivity ratio ρ_{RT}/ρ_0 (ρ_{RT}: the resistivity at

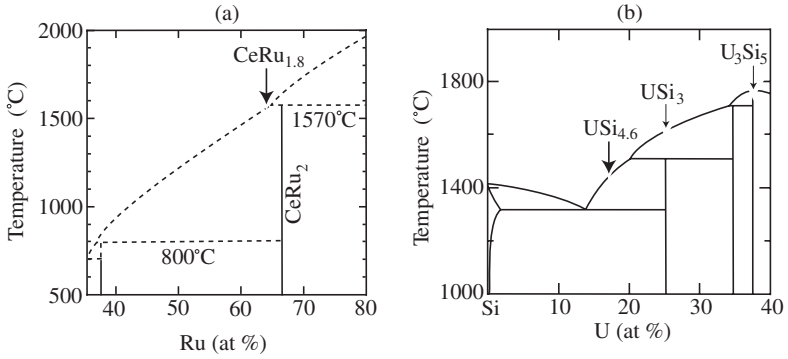

Figure 4. Binary phase diagrams of (a) $CeRu_2$ and (b) USi_3.

room temperature) are 0.25 $\mu\Omega$ cm and 490 in $CeRu_2Si_2$, 0.18 $\mu\Omega$ cm and 680 in UPt_3 and 1.40 $\mu\Omega$ cm and 104 in UPd_2Al_3. In the dHvA experiments, we can estimate the mean free path l for a circular Fermi surface from the following relations: $S_F = \pi k_F^2$, $\hbar k_F = m_c^* v_F$, $T_D = (\hbar/2\pi k_B)\tau^{-1}$ and $l = v_F\tau$, where k_F is the caliper length of S_F and v_F is the Fermi velocity. For example, $l = 1200$ Å in UPt_3 is larger by one order than the coherence length $\xi = 120$ Å in superconductivity. For this high-quality single crystal of UPt_3, the NMR Knight shift experiments were done, clarifying that the superconductivity is of odd parity [11].

The Czochralski method was also applied to the incongruent compounds such as $CeRu_2$ and USi_3. Figure 4 is the binary phase diagram of $CeRu_2$ and USi_3. For these compounds, we prepared the off-stoichiometric starting materials of $CeRu_{1.8}$ and $USi_{4.6}$ in the tetra-arc furnace. Large single-crystal ingots 3–4 mm in diameter and 60 mm in length for $CeRu_2$ and USi_3 were grown, as shown in figure 3(b) for $CeRu_2$. Annealing of the electrotransport method was also applied to the ingot, reaching the residual resistivity $\rho_0 = 0.6$ $\mu\Omega$ cm and the residual resistivity ratio 270 in $CeRu_2$. A very unique dHvA oscillation was detected for the present sample of $CeRu_2$ [12], as shown in figure 5(a). The dHvA oscillation was observed far below $H_{c2} = 52$ kOe, down to a low field of 18 kOe or 0.3 H_{c2}.

The dHvA oscillations are usually observed in the normal state under high-field conditions as mentioned above. This phenomenon was, however, observed even in the superconducting mixed state of $CeRu_2$ as well as $CeCoIn_5$, URu_2Si_2 and UPd_2Al_3 [5, 7, 13], as shown in figure 5. The main Fermi surface named α_i in $CeCoIn_5$ was detected in magnetic fields close to H_{c2}. Surprisingly, a small Fermi surface in $CeRu_2$, URu_2Si_2 and UPd_2Al_3 was detected in low fields down to $H/H_{c2} = 0.3$–0.5. It is questionable whether the small Fermi surface has a superconducting energy gap in magnetic fields far below H_{c2}. This might indicate the growth of a pair-breaking effect far below H_{c2} for the small Fermi surface. More importantly, there is a possibility that the superconducting state for the small Fermi surface is changed into a normal state far below H_{c2}.

In the case of a ferromagnet UIr with a Curie temperature $T_C = 46$ K, the binary phase diagram is extremely complicated. Nevertheless, we succeeded in growing a high-quality single crystal with the residual resistivity 0.5 $\mu\Omega$ cm and the residual resistivity ratio 200 [14]. Recently we observed superconductivity in a critical pressure region [15]. The Curie temperature $T_C = 46$ K is reduced to zero at 1.7 GPa but another magnetic ordering with a ferromagnetic component along the $[10\bar{1}]$ direction appears above 1.9 GPa. The magnetic ordering temperature in the second magnetic phase also becomes zero around 2.6–2.7 GPa, where superconductivity sets in below 0.14 K. In the paramagnetic state above 2.9 GPa, superconductivity disappears completely.

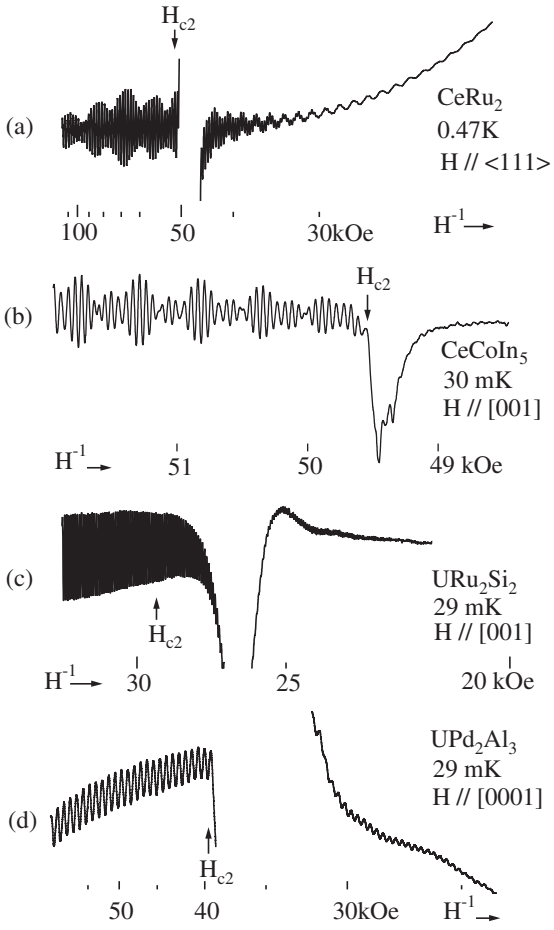

Figure 5. dHvA oscillations in the superconducting mixed states of $CeRu_2$, $CeCoIn_5$, UPd_2Al_3 and URu_2Si_2.

It is noted that the present superconductivity is unique because the crystal structure is of the monoclinic PbBi type, which lacks inversion symmetry (space group $P2_1$, $a = 5.62$ Å, $b = 10.59$ Å, $c = 5.60$ Å, $\beta = 98.9°$), as shown in figure 6. The magnetic moment of $0.5\mu_B$/U is oriented along $[10\bar{1}]$, as shown in figures 6 and 7(a) [16]. The other directions correspond to the hard axes in magnetization, indicating an Ising-like magnetization. This compound indicates the Curie–Weiss law with effective moments of $5f^2$ or $5f^3$ configuration at high temperatures, 3.6 μ_B/U, as shown in figure 7(b). The saturation moment of 0.5 μ_B/U is, however, small, most likely indicating 5f-itinerant-band magnetism, similar to UGe_2 [17].

Figure 8 shows the angular dependence of the dHvA frequency in UIr. The dHvA branches are detected along the [010] direction (b-axis), reflecting the crystal structure. Namely, the crystal structure is elongated along the b-axis, which brings about a flat Brillouin zone along the b-axis, most likely producing cylindrical but highly corrugated Fermi surfaces along the b-axis. The cyclotron mass is relatively large, ranging from 10 to 30 m_0, consistent with the electronic specific heat coefficient $\gamma = 49$ mJ K^{-2} mol^{-1}.

The tetra-arc furnace is useful for the crystal growth of compounds with a high-temperature melting point $T_m \simeq 2000\,°C$. We succeeded in growing high-melting-point compounds such as UC ($T_m = 2630\,°C$), UB_2 ($T_m = 2385\,°C$), UB_4 ($T_m = 2495\,°C$) and $CeRh_3B_2$, where the melting point of $CeRh_3B_2$ is unknown but is estimated to be above 2000 °C. Among these

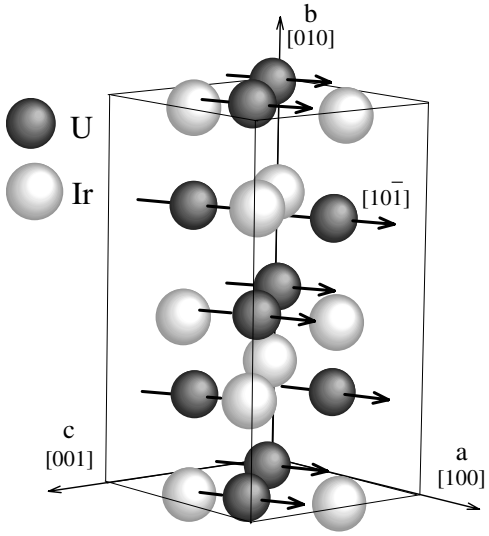

Figure 6. Crystal structure of UIr. The magnetic moment is directed along [10$\bar{1}$].

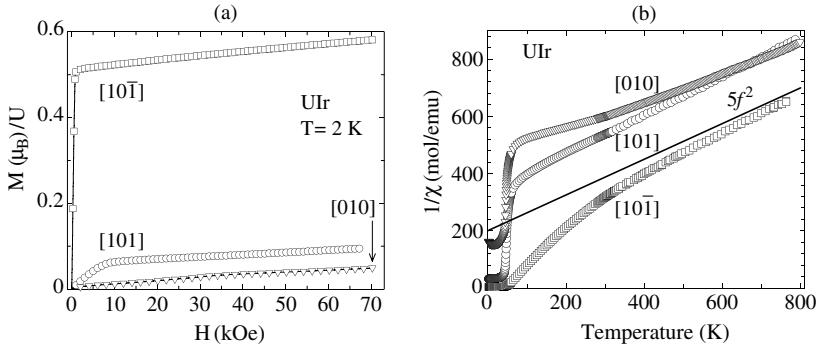

Figure 7. (a) Magnetization and (b) the temperature dependence of the inverse magnetic susceptibility in UIr.

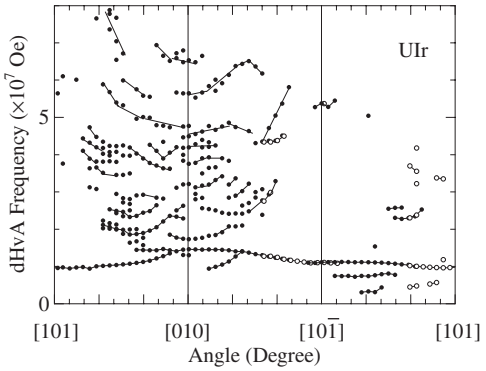

Figure 8. Angular dependence of the dHvA frequency in UIr.

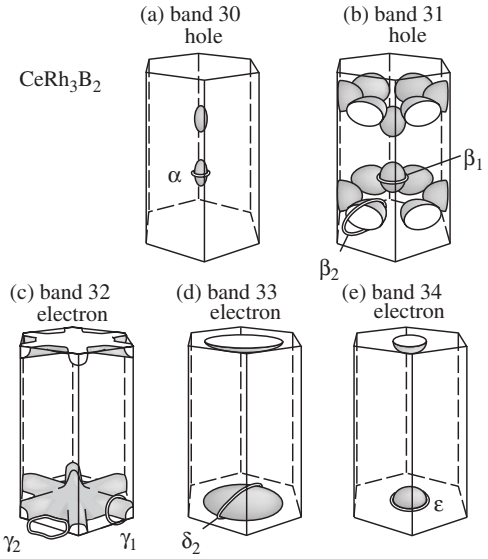

Figure 9. Fermi surfaces with a quasi-one-dimensional character in $CeRh_3B_2$.

compounds, $CeRh_3B_2$ is a unique compound with the highest Curie temperature $T_C = 120$ K in the cerium compounds. Surprisingly, the Curie temperature $T_C = 120$ K is far above $T_C = 91$ K in $GdRh_3B_2$. This means $T_C = 120$ K in $CeRh_3B_2$ is higher by two orders of magnitude than the magnetic ordering temperature expected from the de Gennes factor scaling. An ordered magnetic moment of 0.4 μ_B/Ce, which is oriented along the $[10\bar{1}0]$ direction of the hexagonal structure, is small compared to the usual value of about 1 μ_B/Ce.

We have carried out the dHvA experiments on a ferromagnet $CeRh_3B_2$ and a non-4f reference compound $LaRh_3B_2$ [18]. The dHvA data of $LaRh_3B_2$ are well explained by the results of energy band calculations. Flat Fermi surfaces are realized in $LaRh_3B_2$. This is because the lattice constant along the *c*-axis ([0001] direction) is very short, which enhances the quasi-one-dimensional (1D) conductivity along the *c*-axis. The topology of the Fermi surfaces in $CeRh_3B_2$ is found to be experimentally very similar to that of $LaRh_3B_2$, possessing wavy but flat Fermi surfaces in the basal plane, as shown in figure 9, which was obtained experimentally on the basis of the Fermi surface of $LaRh_3B_2$. The observation of quasi-1D electronic states in these two compounds is the first case in the rare earth compounds.

2.2. Flux method

The flux method is also a useful technique for a high-vapour-pressure case of the melt. In particular, the compounds containing Zn, Cd, Al, Ga, In, Sn, Pb, Sb and Bi metals are grown as single crystals by the so-called self-flux method. Figure 10 shows the U–Sb binary phase diagram. Starting materials with USb_{14} were set in a crucible, as shown by an arrow in figure 10. The temperature was heated up to 1050 °C and cooled down to 600 °C with a rate of 0.5 °C h^{-1}. Many pieces of single crystals of $10 \times 10 \times 5$ mm^3 were grown, as shown in the inset. Excess antimony was removed by using a centrifuge.

Uranium dipnictides UX_2 (X: Bi, Sb, As and P) crystallize in the tetragonal structure of anti-Cu_2Sb type (D^7_{4h} of $P4/nmm$). They order antiferromagnetically. The magnetic moments of uranium ions are aligned ferromagnetically in the (001) planes, which are stacked along the [001] direction in an antiferromagnetic (↑↓) sequence in UBi_2. In the case of USb_2, UAs_2 and UP_2, this sequence is (↑↓↓↑). It is worth mentioning here that the magnetic unit cell of USb_2,

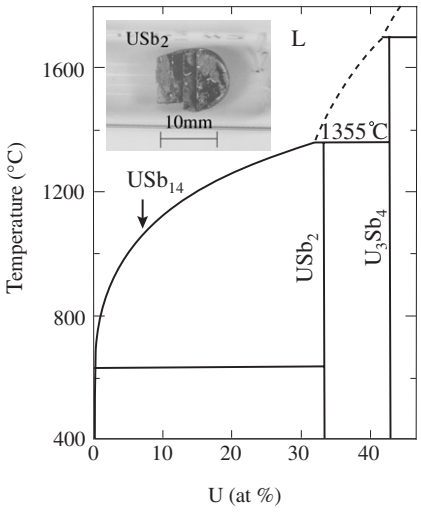

Figure 10. U–Sb binary phase diagram. The inset shows the USb_2 single crystal.

UAs_2 and UP_2 is doubled with respect to the chemical unit cell along [001], which brings about a flat magnetic Brillouin zone.

We have studied the Fermi surface properties from the dHvA experiments. The Fermi surface of UBi_2 is found to consist of one spherical hole Fermi surface and two cylindrical electron Fermi surfaces. For USb_2 with $T_N = 203$ K, we observed a quasi-two-dimensional Fermi surface [19]. Namely, each Fermi surface in UBi_2 splits into two cylindrical Fermi surfaces in USb_2, which are well explained by the band-folding procedure in a flat magnetic Brillouin zone. The quasi-2D character of these Fermi surfaces is mainly due to the conduction electrons in the U plane, including the 5f electrons, because the cyclotron masses of compensated electron and hole carriers are moderately large, ranging from 2.0 to 6.0 m_0.

Quasi-2D Fermi surfaces were observed in $CeAgSb_2$ [20], $CeTIn_5$ (T: Co, Rh, Ir) [21], $UTGa_5$ (T: Fe, Ni, Pt) [21, 22] and CePtX (X: P, As) [23] compounds. Among them, $CeCoIn_5$ with the tetragonal structure is typical in the Fermi surface properties. $CeTIn_5$, $UTGa_5$ and $PuTGa_5$ (T: transition metal) crystallize in the same tetragonal crystal structure. In $CeTIn_5$, uniaxially distorted $AuCu_3$-type layers of $CeIn_3$ and the TIn_2 layers are stacked sequentially along the [001] direction (c-axis). The d electrons in the T atom hybridize with the 5p electrons of In in $CeTIn_5$, which results in a small density of states around the Fermi energy. This means that there are very few conduction electrons in the TIn_2 layer and hence the Fermi surface mainly consists of two kinds of cylindrical Fermi surfaces.

Figure 11 shows the field dependence of the cyclotron mass for branches α_i and β_i and their cylindrical Fermi surfaces. Both Fermi surfaces are mainly of 4f-electron character. Branch β_i (band 14-electron Fermi surface) is expected to possess a cyclotron mass of 100 m_0 at low fields, while branch α_i possesses the cyclotron mass of 15–30 m_0. It has been pointed out theoretically that the magnetically mediated pairing is more robust for the nearly antiferromagnetic system (for example, a spin-singlet $d_{x^2-y^2}$ state) than for the ferromagnetic one (a spin-triplet p-wave state) and is more favourable in the quasi-two-dimensional than three-dimensional systems [24].

Here we note the superconducting transition temperature T_{sc}. $PuCoGa_5$ is a superconductor with a large T_{sc} value of 18.5 K and a relatively large γ value of $\gamma = 77$ mJ K^{-2} mol^{-1} [25]. This γ value is smaller by one order of magnitude than that of $CeCoIn_5$. Therefore a relatively large band width, together with two dimensionality, probably enhances the superconducting

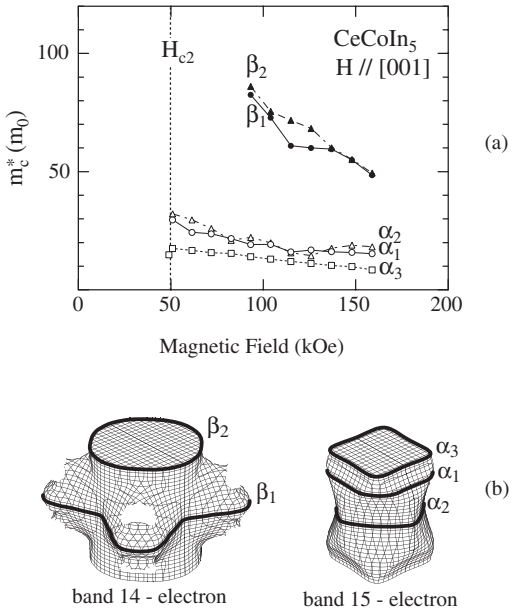

Figure 11. (a) Field dependence of the cyclotron mass for branches α_i and β_i and (b) the corresponding main cylindrical Fermi surfaces in $CeCoIn_5$.

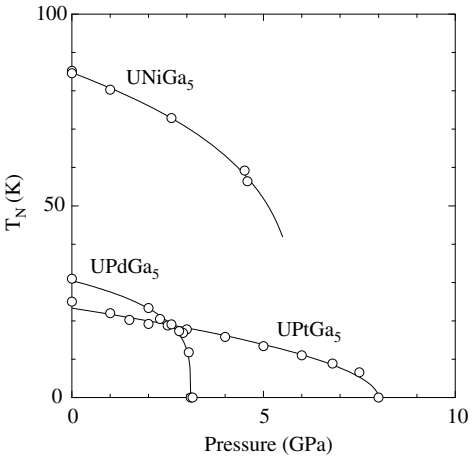

Figure 12. Pressure dependence of the Néel temperature for $UNiGa_5$, $UPdGa_5$ and $UPtGa_5$.

transition temperature in $PuCoGa_5$. It is interesting to note the T_{sc} values: $T_{sc} = 0.22$ K in $CeIn_3$ under 2.7 GPa with a three-dimensional Fermi surface, 2.3 K in $CeCoIn_5$ and 18.5 K in $PuCoGa_5$. The correlation of T_{sc} with the band width can be extended to a large T_{sc} value of high-T_{sc} cuprates, where the itinerant 3d electrons in the CuO_2 plane are responsible for superconductivity. We also note the electronic states of $UCoGa_5$. It is a Pauli paramagnet and possesses small closed Fermi surfaces, indicating a semimetal [21]. This is a reason why superconductivity is not realized in $UCoGa_5$.

There is, however, a possibility of pressure-induced superconductivity in antiferromagnets $UTGa_5$ (T: Ni, Pd and Pt). For example, Fermi surfaces of $UPtGa_5$ are quasi-two-dimensional. Four kinds of cylindrical Fermi surfaces with 10–24m_0 were observed in the dHvA experiments [22]. Figure 12 shows the pressure dependence of the Néel temperature for $UNiGa_5$ (a Néel temperature $T_N = 86$ K, an ordered moment $\mu = 0.90\mu_B$/U), $UPdGa_5$

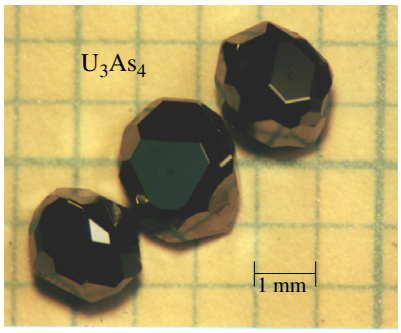

(a)

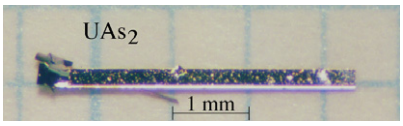

(b)

Figure 13. Single crystals of (a) U_3As_4 and (b) UAs_2.

($T_N = 31$ K, $\mu = 0.33\ \mu_B$/U) and $UPtGa_5$ ($T_N = 26$ K, $\mu = 0.26\mu_B$/U). The Néel temperature decreases with increasing pressure and becomes zero at a critical pressure $P_c = 6$–7 GPa in $UNiGa_5$, $P_c = 3$ GPa in $UPdGa_5$ and $P_c = 8$ GPa in $UPtGa_5$. We are now searching for superconductivity around P_c for these compounds.

2.3. Chemical transport method with iodine

In the extremely-high-vapour-pressure case of the melt, a chemical transport method using iodine vapour is useful for the compounds containing P, As, S, Se and Te elements. Figure 13 shows a photograph of U_3As_4 and UAs_2 single crystals. The stoichiometric amounts of U and As in U_3As_4 were sealed together with 3 mg cm^{-3} iodine in an evacuated quartz ampoule. The ampoule was gradually heated and retained at 950 °C for four days until pre-reaction of U with As was completed. Then the ampoule was placed in the temperature gradient with a hot region at 925 °C and a hotter region at 975 °C for two weeks. Many but small single crystals were grown on the wall of the ampoule.

The dHvA experiments were done for U_3As_4 as well as U_3P_4 [26]. The cyclotron effective mass of the detected Fermi surfaces is large, ranging from 5 to 70 m_0. High-pressure experiments using a diamond anvil cell were also done for U_3P_4 [27]. The Curie temperature $T_C = 138$ K decreases with increasing pressure and becomes zero at $P_c = 5$ GPa. The coefficient A of the resistivity $\rho = \rho_0 + AT^2$ becomes maximum at P_c: $A = 0.05\ \mu\Omega$ cm K^{-2} at ambient pressure and 0.92 $\mu\Omega$ cm K^{-2} at 5 GPa. Superconductivity was, however, not observed in this compound down to 0.1 K. It is noted that the crystal structure (T_d^6 or $I\bar{4}3d$) lacks inversion symmetry.

2.4. Bridgman method

The Bridgman method is useful in the same high-vapour-pressure case of the melt, and also for the incongruent compounds. For example, in the case of a new heavy-fermion superconductor $CePt_3Si$, the Czochralski and Bi- and Sn-flux methods were not useful in growing a single crystal because this compound is an incongruent compound. The Bridgman and/or mineralization methods were applied to it. The starting materials were arc-melted, sealed in a Mo crucible. The crucible was heated up to 1450 °C and cooled down gradually.

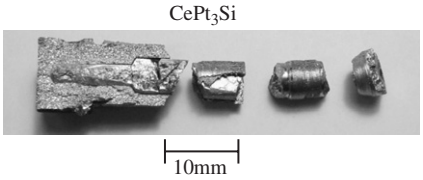

Figure 14. Cross-section of the single-crystal ingot of $CePt_3Si$ in a Mo crucible.

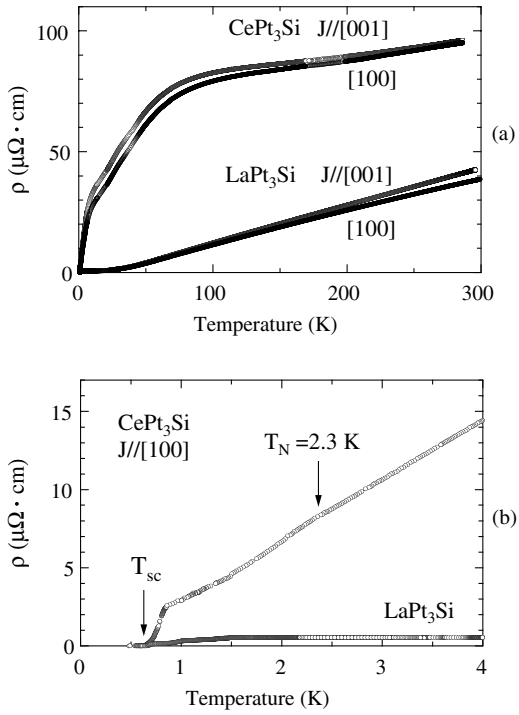

Figure 15. Temperature dependence of the electrical resistivity in $CePt_3Si$ and $LaPt_3Si$.

Figure 14 shows the cross-section of a single-crystal ingot of $CePt_3Si$ in the Mo crucible. We show in figure 15 the temperature dependence of the electrical resistivity in $CePt_3Si$ and $LaPt_3Si$ single crystals. The electrical resistivity for $J \parallel [100]$ and [001] is almost the same, indicating the 3D electronic states in $CePt_3Si$ and $LaPt_3Si$. Both compounds become superconductive below 0.6–0.7 K.

$CePt_3Si$ is unique, possessing a few characteristics [28]. Superconductivity is realized in the long-range antiferromagnetic ordering. The Néel temperature is 2.2 K, while the superconducting transition temperature is 0.75 K. Both transitions were observed clearly in the specific heat measurement. The electronic specific heat coefficient γ is large, 300–400 mJ K^{-2} mol^{-1}. Moreover, $CePt_3Si$ lacks a centre of symmetry in the tetragonal structure ($P4mm$). The existence of inversion symmetry in the crystal structure is believed to be a favourable factor for superconductivity. The absence of superconductivity in, for example, a ferromagnet MnSi [29] or U_3P_4 mentioned above has been tentatively attributed to a lack of inversion symmetry. Theoretical considerations are needed to clarify the relation between superconductivity and lack of inversion symmetry for $CePt_3Si$ and also UIr.

3. Concluding remarks

We have presented the unique electronic states, focusing on the quasi-2D electronic states, which are closely related to the crystal structure elongated along the c-axis in the tetragonal or hexagonal structures. It was clarified experimentally and theoretically that the superconducting transition temperature in the quasi-2D compounds, for example $T_{sc} = 2.3$ K in $CeCoIn_5$, is enhanced compared to that in the 3D compounds, 0.2 K in $CeIn_3$ under 2.7 GPa. The quasi-2D electronic states are also found to be formed by the flat magnetic Brillouin zone as in USb_2.

In the magnetically ordered uranium compounds, the 5f electrons contribute to the volume of the Fermi surface and also to the magnetic moment of the uranium site, possessing a dual nature. We presented that the Fermi surface in UPd_2Al_3 is well explained by the spin-polarized 5f-itinerant-band model. This model is also applicable to an antiferromagnet $UPtGa_5$, but not applicable to all the magnetically ordered uranium compounds. For example, the dHvA data of a ferromagnet UGa_2 ($T_C = 124$ K, a saturation moment 3.0 μ_B/U) are explained by neither the spin-polarized 5f-itinerant-band model nor the 5f-localized-band model [30]. It is noted that the 5f-localized-band model is applicable to the dHvA data of an antiferroquadrupolar compound, UPd_3 [31], where the 5f electrons are clarified to be localized from the neutron scattering experiment. On the other hand, the conventional 5f-itinerant-band model is well applicable to the non-magnetic uranium compounds including UPt_3. For the magnetically ordered uranium compounds, it is furthermore needed to study the Fermi surface property experimentally and theoretically.

In the non-magnetic cerium compounds including $CeRu_2Si_2$ and $CeCoIn_5$, it is also clarified that the dHvA data are well explained by the 4f-itinerant-band model. On the other hand, the 4f electron in the magnetically ordered cerium compounds does not contribute to the volume of the Fermi surface but to the magnetic moment at the cerium site. In an antiferromagnet $CeRh_2Si_2$, the nature of the 4f electron was tuned by pressure and it was clarified via the dHvA experiment and the energy band calculation that a discontinuous change of the Fermi surface from 4f localized to itinerant occurs at a critical pressure $P_c \simeq 1.06$ GPa, implying a first-order phase transition [32]. It is now needed to clarify the Fermi surface property of a new heavy-fermion superconductor $CePt_3Si$. In $CePt_3Si$, together with UIr, many experimental and theoretical studies are needed to clarify superconductivity without space inversion symmetry.

Acknowledgments

We are very grateful to Drs N Kimura, M Hedo, D Aoki, Y Tokiwa, S Araki, M Nakashima, S Ikeda and H Shishido for collaboration. The present work was financially supported by a Grant-in-Aid for Scientific Research COE (10CE2004) and Creative Scientific Research (15GS0123).

References

[1] Ōnuki Y, Goto T and Kasuya T 1991 *Materials Science and Technology* vol 3A, ed K H J Buschow (Weinheim: VCH) part I, chapter 7, p 545
[2] Ōnuki Y and Hasegawa A 1995 *Handbook on the Physics and Chemistry of Rare Earth* vol 20, ed K A Gschneidner Jr and L Eyring (Amsterdam: Elsevier Science) p 1
[3] Haga Y, Yamamoto E, Tokiwa Y, Aoki D, Inada Y, Settai R, Maehira T, Yamagami H, Harima H and Ōnuki Y 2002 *J. Nucl. Sci. Technol. Suppl.* **3** 56
[4] Aoki H, Uji S, Albessard A K and Ōnuki Y 1993 *Phys. Rev. Lett.* **71** 2110

[5] Settai R, Shishido H, Ikeda S, Murakawa Y, Nakashima M, Aoki D, Haga Y, Harima H and Ōnuki Y 2001 *J. Phys.: Condens. Matter* **13** L627
[6] Kimura N, Tani T, Aoki H, Komatsubara T, Uji S, Aoki D, Inada Y, Ōnuki Y, Haga Y, Yamamoto E and Harima H 2000 *Physica* B **281/282** 710
[7] Inada Y, Yamagami H, Haga Y, Sakurai K, Tokiwa Y, Honma T, Yamamoto E, Ōnuki Y and Yanagisawa T 1999 *J. Phys. Soc. Japan* **68** 3643
[8] Knöpfle K, Mavromaras A, Sandratskii L M and Kübler J 1996 *J. Phys.: Condens. Matter* **8** 901
[9] Haga Y, Honma T, Yamamoto E, Ohkuni H, Ōnuki Y, Ito Y M and Kimura N 1998 *Japan. J. Appl. Phys.* **37** 3604
[10] Shimizu K, Kimura T, Furomoto S, Takeda K, Kantani K, Ōnuki Y and Amaya K 2001 *Nature* **412** 316
[11] Tou H, Kitaoka Y, Ishida K, Asayama K, Kimura N, Ōnuki Y, Yamamoto E, Haga Y and Maezawa K 1998 *Phys. Rev. Lett.* **80** 3129
[12] Hedo M, Inada Y, Sakurai K, Yamamoto E, Haga Y, Ōnuki Y, Takahashi S, Higuchi M, Maehira T and Hasegawa A 1998 *Phil. Mag.* B **77** 475
[13] Inada Y and Ōnuki Y 1999 *Low Temp. Phys.* **25** 573
[14] Yamamoto E, Haga Y, Matsuda T D, Nakamura A, Settai R, Inada Y, Sugawara H, Sato H and Ōnuki Y 2002 *J. Nucl. Sci. Technol. Suppl.* **3** 187
[15] Akazawa T, Hidaka H, Fujiwara T, Kobayashi T C, Yamamoto E, Haga Y, Settai R and Ōnuki Y 2004 *J. Phys.: Condens. Matter* **16** L29
[16] Galatanu A, Haga Y, Yamamoto E, Matsuda T D, Ikeda S and Ōnuki Y 2004 *J. Phys. Soc. Japan* **73** 766
[17] Settai R, Nakashima M, Araki S, Haga Y, Kobayashi T C, Tateiwa N, Yamagami H and Ōnuki Y 2002 *J. Phys.: Condens. Matter* **14** L29
[18] Okubo T, Yamada M, Thamizhavel A, Kirita S, Inada Y, Settai R, Harima H, Takegahara K, Galatanu A, Yamamoto E and Ōnuki Y 2003 *J. Phys.: Condens. Matter* **15** L721
[19] Aoki D, Wiśniewski P, Miyake K, Watanabe N, Inada Y, Settai R, Yamamoto E, Haga Y and Ōnuki Y 2000 *Phil. Mag.* B **80** 1517
[20] Inada Y, Thamizhavel A, Yamagami H, Takeuchi T, Sawai Y, Ikeda S, Shishido H, Okubo T, Yamada M, Sugiyama K, Nakamura N, Yamamoto T, Kindo K, Ebihara T, Galatanu A, Yamamoto E, Settai R and Ōnuki Y 2002 *Phil. Mag.* B **82** 1867
[21] Ōnuki Y, Aoki D, Wiśniewski P, Shishido H, Ikeda S, Inada Y, Settai R, Tokiwa Y, Yamamoto E, Haga Y, Maehira T, Harima H, Higuchi M, Hasegawa A and Yamagami H 2001 *Acta Phys. Pol.* B **32** 3273
[22] Ikeda S, Tokiwa Y, Haga Y, Yamamoto E, Ōkubo T, Yamada M, Nakamura N, Sugiyama K, Kindo K, Inada Y, Yamagami H and Ōnuki Y 2003 *J. Phys. Soc. Japan* **72** 576
[23] Settai R, Yoshida Y, Yamagami A, Ōnuki Y, Yoshii S, Kasaya M, Harima H and Takegahara K 1999 *J. Phys. Soc. Japan* **68** 3615
[24] Monthoux P 2003 *J. Phys.: Condens. Matter* **15** S1973
[25] Sarrao J L, Morales L A, Thompson J D, Scott B L, Stewart G R, Wastin F, Reblzant J, Boulet P and Collneau E 2002 *Nature* **420** 297
[26] Inada Y, Wiśniewski P, Murakawa M, Aoki D, Miyake K, Watanabe N, Haga Y, Yamamoto E and Ōnuki Y 2001 *J. Phys. Soc. Japan* **70** 558
[27] Takeda K, Tanaka T, Kobayashi T C, Akazawa T, Shimizu K, Amaya K, Inada Y, Wiśniewski P, Aoki D, Yamamoto E, Haga Y and Ōnuki Y 2002 *J. Nucl. Sci. Technol. Suppl.* **3** 191
[28] Bauer E, Hilscher G, Michor H, Paul Ch, Scheidt E W, Gribanov A, Seropegin Yu, Noël H, Sigrist M and Rogl P 2004 *Phys. Rev. Lett.* **92** 027003
[29] Pfleiderer C, McMullan G J, Julian S R and Lonzarich G G 1997 *Phys. Rev.* B **55** 8330
[30] Honma T, Inada Y, Settai R, Araki S, Tokiwa Y, Takeuchi T, Sugawara H, Sato H, Kuwahara K, Yokoyama M, Amitsuka H, Sakakibara S, Yamamoto E, Haga Y, Nakamura A, Harima H, Yamagami H and Ōnuki Y 2000 *J. Phys. Soc. Japan* **69** 2647
[31] Tokiwa Y, Sugiyama K, Takeuchi T, Nakashima M, Settai R, Inada Y, Haga Y, Yamamoto E, Kindo K, Harima H and Ōnuki Y 2001 *J. Phys. Soc. Japan* **70** 1731
[32] Araki S, Settai R, Nakashima M, Shishido H, Ikeda S, Nakawaki H, Haga Y, Tateiwa N, Kobayashi T C, Harima H, Yamagami H, Aoki Y, Namiki T, Sato H and Ōnuki Y 2002 *J. Phys. Chem. Solids* **63** 1133